**SPACE MAPPING OPTIMIZATION OF MICROWAVE CIRCUITS
EXPLOITING SURROGATE MODELS**

M.H. Bakr, J.W. Bandler, K. Madsen, J.E. Rayas-Sánchez and J. Søndergaard

SOS-00-12-R

(Revised August 2000)

SPACE MAPPING OPTIMIZATION OF MICROWAVE CIRCUITS
EXPLOITING SURROGATE MODELS

M.H. Bakr, *Student Member*, *IEEE*, J.W. Bandler, *Fellow*, *IEEE*, K. Madsen, J.E. Rayas-Sánchez, *Senior Member*, *IEEE*, and J. Søndergaard

Abstract   A powerful new Space Mapping (SM) optimization algorithm is presented. It draws upon recent developments in both surrogate model-based optimization and modeling of microwave devices. SM optimization is formulated as a general optimization problem of a surrogate model. This model is a convex combination of a mapped coarse model and a linearized fine model. It exploits, in a novel way, a linear frequency-sensitive mapping. During the optimization iterates, the coarse and fine models are simulated at different sets of frequencies. This approach is shown to be especially powerful if a significant response shift exists. The algorithm is illustrated through the design of a capacitively-loaded 10-1 impedance transformer and a Double-Folded Stub (DFS) filter.   A High-Temperature Superconducting (HTS) filter is also designed using decoupled frequency and space mappings.

I. INTRODUCTION

In this work we present a novel Space Mapping (SM) algorithm for microwave circuit optimization [1]. It integrates, for the first time, two distinct optimization approaches: SM optimization [2-4] and surrogate model-based optimization [5-7]. Both approaches aim at efficiently optimizing an

M.H. Bakr, J.W. Bandler and J.E. Rayas-Sánchez are with the Simulation Optimization Systems Research Laboratory and the Department of Electrical and Computer Engineering, McMaster University, Hamilton, Ontario, Canada, L8S 4K1.

J.W. Bandler is also with Bandler Corporation, P.O. Box 8083, Dundas, Ontario, Canada L9H 5E7.

K. Madsen and J. Søndergaard are with the Department of Mathematical Modelling, Technical University of Denmark, DK-2800 Lyngby, Denmark.

accurate and time-intensive "fine" model, e.g., a full-wave electromagnetic (EM) simulator. SM exploits the existence of a less accurate but fast "coarse" model. It formulates the design problem as a system of nonlinear equations. On the other hand, surrogate-based optimization, new to the microwave arena, exploits an approximate model in iteratively solving the original design problem. This model may be a less accurate physically-based model or algebraic model [6].

Our algorithm combines both approaches. The original design problem is iteratively solved using a surrogate model. This model is a convex combination of a mapped coarse model and a linearized fine model. The accuracy of the surrogate model is improved in every iteration using the generated fine model simulations.

Recent developments in Space Mapping-based Neuromodeling (SMN) [8] and Generalized Space Mapping (GSM) modeling [9] exploit frequency-sensitive mappings. This approach is reported to improve the accuracy of SM-based models. We integrate this concept, in a novel way, with SM optimization. In each iteration, a linear frequency-sensitive mapping is exploited in constructing the mapped coarse model. Here, the coarse and fine models are simulated over different frequency ranges. This approach handles significant frequency shifts efficiently.

The established frequency-sensitive mapping obtains an estimate of the derivatives of the mapped coarse model responses. These derivatives are expressed in terms of the coarse model derivatives and the mapping parameters. We show that this expression is a generalized form for frequency-sensitive mappings of the lemma utilized in [4]. It can be used to approximate the fine model derivatives in the region of interest.

A number of examples are successfully solved. They include a capacitively-loaded two-section 10:1 impedance transformer [10], a Double-Folded Stub (DFS) filter [11] and a High Temperature Superconducting (HTS) filter [12]. Decoupled frequency and space mappings are utilized in the optimization of the HTS filter. This approach shows the feasibility of utilizing different types of frequency-sensitive mappings in the optimization loop.

II. SPACE MAPPING OPTIMIZATION VS. SURROGATE-BASED OPTIMIZATION

We denote the fine model responses at a point $x_f \in \Re^{n \times 1}$ and frequency ω by $R_f(x_f, \omega) \in \Re^{N_r \times 1}$. These responses may include the real and imaginary parts of S_{11}, etc. The vector $R_f(x_f) \in \Re^{m \times 1}$ denotes the responses at all the N_ω simulation frequencies where $m = N_r N_\omega$. The original design problem is

$$x_f^* = arg \left\{ \begin{array}{l} min \\ x_f \end{array} U(R_f(x_f)) \right\} \tag{1}$$

where U is the objective function and x_f^* is the optimal fine model design. Solving (1) using direct optimization methods, e.g. [13], is prohibitive due to the intensive simulation time of the fine model.

SM optimization exploits the existence of a fast but less accurate "coarse" model of the circuit. We denote by $x_c \in \Re^{n \times 1}$ and $R_c(x_c) \in \Re^{m \times 1}$ a coarse model point and the corresponding coarse model response vector, respectively. The coarse model responses at a frequency ω_c are similarly denoted by $R_c(x_c, \omega_c) \in \Re^{N_r \times 1}$.

The first step in all SM-based optimization algorithms obtains the optimal coarse model design x_c^*. The corresponding response is denoted by $R_c^* \in \Re^{m \times 1}$. SM aims at establishing a mapping P between the two spaces [2]

$$x_c = P(x_f) \tag{2}$$

such that

$$R_f(x_f) \approx R_c(x_c) \tag{3}$$

over a region in the parameter space. SM optimization obtains a space-mapped design $\overline{x}_f$ whose response matches R_c^*. $\overline{x}_f$ is a solution of the nonlinear system

3

$$f(x_f) = P(x_f) - x_c^* = 0 \tag{4}$$

where $P(x_f)$ is approximated through a Parameter Extraction (PE) procedure.

Previous SM optimization algorithms [2-4] solve (4) iteratively. Let $x_f^{(i)}$ be the ith iterate. Aggressive Space Mapping (ASM) [2] predicts a new iterate $x_f^{(i+1)} = x_f^{(i)} + h^{(i)}$ by utilizing the quasi-Newton iteration

$$B^{(i)} h^{(i)} = -f(x_f^{(i)}) \tag{5}$$

$B^{(i)}$ is an approximation to the Jacobian of f with respect to x_f at $x_f^{(i)}$. It is updated at the end of every iteration using Broyden's update [14].

The Trust Region Aggressive Space Mapping (TRASM) algorithm [3] minimizes $\left\| f(x_f^{(i+1)}) \right\|$ using least squares within a trust region. The ith iteration of the algorithm is given by

$$(B^{(i)T} B^{(i)} + \psi I) h^{(i)} = -B^{(i)T} f^{(i)} \tag{6}$$

Parameter ψ is selected such that $\left\| h^{(i)} \right\| \leq \delta^{(i)}$, where $\delta^{(i)}$ is the size of the trust region. The new iterates are accepted only if they are descent directions for $\left\| f \right\|$. TRASM also utilizes a recursive multi-point extraction procedure to enhance the uniqueness of PE.

Hybrid Aggressive Space Mapping (HASM) [4] addresses the problem of a poor coarse model. It adopts a two phase approach. The first phase exploits a TRASM strategy. The second phase minimizes $\left\| R_f(x_f) - R_c^* \right\|_2$ through direct least-squares optimization. A relationship relates the available mapping to the first-order derivatives of the responses of both models [4]. It is used for switching between the two phases.

Alternatively, an expensive model can be optimized indirectly by using a surrogate model [5-7]. This surrogate model may be a less accurate physics-based model or a polynomial approximation of the

fine model [6]. We denote the surrogate model in the ith iteration by $R_s^{(i)}(x_f) \in \Re^{m \times 1}$. The ith iteration step is obtained by solving

$$h^{(i)} = arg \left\{ \min_{h^{(i)}} U(R_s^{(i)}(x_f^{(i)} + h^{(i)})) \right\}, \ \left\| h^{(i)} \right\| \le \delta^{(i)} \qquad (7)$$

where $U(R_s^{(i)}(x_f^{(i)} + h^{(i)}))$ is the value of the objective function evaluated using the surrogate model at the point $x_f^{(i)} + h^{(i)}$. The point $x_f^{(i)} + h^{(i)}$ is then validated using fine model simulation. It is accepted if it improves the fine model objective function. Otherwise, the accuracy of $R_s^{(i)}(x_f)$ should be improved. Different strategies can be utilized for improving the surrogate model accuracy. One strategy utilizes only the validation fine model simulations. Additional fine simulations may be generated to improve the surrogate model in certain directions of the parameter space

III. THE SURROGATE MODEL

In the ith iteration, our algorithm utilizes a surrogate model expressed as a convex combination of a Linearized Fine Model (LFM) and a Mapped Coarse Model (MCM) $R_m^{(i)}(x_f)$. It is given by

$$R_s^{(i)}(x_f) = \lambda^{(i)} R_m^{(i)}(x_f) + (1 - \lambda^{(i)})(R_f(x_f^{(i)}) + J_f^{(i)} \Delta x_f), \ \lambda^{(i)} \in [0,1] \qquad (8)$$

$J_f^{(i)} \in \Re^{m \times n}$ is an approximation to the Jacobian of fine model responses at $x_f^{(i)}$ and $\Delta x_f = x_f - x_f^{(i)}$. The parameter $\lambda^{(i)}$ determines which model is favored. If $\lambda^{(i)} = 1$, the surrogate model becomes a MCM. If $\lambda^{(i)} = 0$, the surrogate model becomes a LFM. $\forall \lambda^{(i)} \in (0,1)$, the surrogate model exploits both approximations. The LFM part in (8) ensures that the algorithm will work if the coarse model is poor or even wrong.

The MCM $R_m^{(i)}(x_f)$ utilizes the linear frequency-space mapping

$$R_f(x_f, \omega_j) \approx R_m^{(i)}(x_f, \omega_j) = \qquad (9)$$

5

$$\boldsymbol{R}_c(\boldsymbol{P}^{(i)}(\boldsymbol{x}_f,\omega_j),P_\omega^{(i)}(\boldsymbol{x}_f,\omega_j)),\ j{=}1,\,2,\,...,\,N_\omega$$

where

$$\begin{bmatrix}\boldsymbol{P}^{(i)}(\boldsymbol{x}_f,\omega_j)\\P_\omega^{(i)}(\boldsymbol{x}_f,\omega_j)\end{bmatrix}=\begin{bmatrix}\boldsymbol{B}^{(i)}&\boldsymbol{s}^{(i)}\\\boldsymbol{t}^{(i)T}&\sigma^{(i)}\end{bmatrix}\begin{bmatrix}\Delta\boldsymbol{x}_f\\\omega_j\end{bmatrix}+\begin{bmatrix}\boldsymbol{c}^{(i)}\\\gamma^{(i)}\end{bmatrix},\tag{10}$$

The parameters $\boldsymbol{B}^{(i)}\in\Re^{n\times n}$, $\boldsymbol{s}^{(i)}\in\Re^{n\times1}$, $\boldsymbol{t}^{(i)}\in\Re^{n\times1}$, $\boldsymbol{c}^{(i)}\in\Re^{n\times1}$, $\sigma^{(i)}\in\Re^{1\times1}$ and $\gamma^{(i)}\in\Re^{1\times1}$ are the mapping

parameters. ω_j is the jth simulation frequency, $j{=}1,\,2,\,...,\,N_\omega$. Here, a fine model point $\boldsymbol{x}_f$ and

frequency ω_j correspond to a coarse model point $\boldsymbol{P}^{(i)}(\boldsymbol{x}_f,\omega_j)$ and coarse model frequency

$P_\omega^{(i)}(\boldsymbol{x}_f,\omega_j)$. Notice that (10) defaults to the frequency-insensitive mapping utilized by the ASM,

TRASM and HASM algorithms if $\boldsymbol{s}^{(i)}=\boldsymbol{t}^{(i)}=\boldsymbol{0}$, $\sigma^{(i)}=1$ and $\gamma^{(i)}=0$.

The advantage of utilizing (10) is illustrated by Fig. 1. It is required to extract the coarse point

$\boldsymbol{x}_c$ corresponding to a given fine point $\boldsymbol{x}_f$. Previous SM-based algorithms utilize the PE procedure

$$\boldsymbol{x}_c=arg\left\{\min_{\boldsymbol{x}_c}\left\|\boldsymbol{R}_f(\boldsymbol{x}_f)-\boldsymbol{R}_c(\boldsymbol{x}_c)\right\|\right\}\tag{11}$$

Fig. 1(a) shows also the coarse model response at the starting point for (11). The PE optimizer may not

have enough information to align the almost disjoint responses. However, the responses align perfectly if

a frequency transformation $\omega_c=P_\omega(\omega)$ is applied to the coarse model frequency axis. This implies that

the two models are simulated at different frequencies. Fig. 1(b) shows the aligned responses. It follows

that (10) allows another degree of freedom in aligning the coarse and fine models.

Utilizing a frequency sensitive mapping also enables indirect estimation of the fine model

derivatives. Using (9), the Jacobian of the mapped coarse model responses $\boldsymbol{J}_m(\boldsymbol{x}_f^{(k)},\omega_j)\in\Re^{N_r\times n}$ at a

point $\boldsymbol{x}_f^{(k)}$ and frequency ω_j is given by

$$J_m(x_f^{(k)}, \omega_j) = \left(\frac{\partial R_m^T(x_f, \omega)}{\partial x_f}\right)^T \Bigg|_{\substack{x_f = x_f^{(k)} \\ \omega = \omega_j}} =$$

$$\left(\frac{\partial P^T}{\partial x_f} \frac{\partial R_c^T(P, P_\omega)}{\partial P} + \frac{\partial P_\omega}{\partial x_f} \frac{\partial R_c^T(P, P_\omega)}{\partial P_\omega}\right)^T \Bigg|_{\substack{P = P^{(i)}(x_f^{(k)}, \omega_j) \\ P_\omega = P_\omega^{(i)}(x_f^{(k)}, \omega_j)}}$$

(12)

For the case of the linear frequency-sensitive mapping (10), relation (12) becomes

$$J_m(x_f^{(k)}, \omega_j) = \left(\left(\frac{\partial R_c^T(P, P_\omega)}{\partial P}\right)^T B^{(i)} + \frac{\partial R_c(P, P_\omega)}{\partial P_\omega} t^{(i)T}\right) \Bigg|_{\substack{P = P^{(i)}(x_f^{(k)}, \omega_j) \\ P_\omega = P_\omega^{(i)}(x_f^{(k)}, \omega_j)}}$$

(13)

Formula (13) utilizes only coarse model derivatives in estimating the MCM derivatives. It defaults to the lemma utilized by the HASM algorithm [4]

$$J_m(x_f^{(k)}, \omega_j) = J_c(P^{(i)}(x_f^{(k)}, \omega_j), P_\omega^{(i)}(x_f^{(k)}, \omega_j)) B^{(i)}$$

(14)

for the case of a linear frequency-insensitive mapping $P^{(i)}(x_f, \omega) = B^{(i)} \Delta x_f + c^{(i)}$ and $P_\omega^{(i)}(x_f, \omega) = \omega$.

The MCM should approximate the fine model over a region of fine model parameters and frequency. The mapping parameters are thus obtained through the optimization procedure

$$[B^{(i)}, s^{(i)}, t^{(i)}, \sigma^{(i)}, c^{(i)}, \gamma^{(i)}] =$$

$$arg\left\{\min_{B, s, t, \sigma, c, \gamma} \; \left\| \; [e_1 \quad e_2 \quad \cdots \quad e_{N_p}]^T \; \right\|\right\}$$

(15)

$$e_k = R_m(x_f^{(k)}) - R_f(x_f^{(k)}) \quad \forall x_f^{(k)} \in V^{(i)},$$

(16)

where $V^{(i)}$ is a set of fine model points whose cardinality is $|V^{(i)}| = N_p$. $V^{(i)}$ is constructed through an iterative process. Initially, we set $V^{(i)} = \{x_f^{(i)}\}$. The two conditions

$$\frac{(x_f - x_f^{(i)})^T (x_f^{(k)} - x_f^{(i)})}{\left\|(x_f - x_f^{(i)})\right\| \left\|x_f^{(k)} - x_f^{(i)}\right\|} \leq 1 - \varepsilon \; \forall x_f^{(k)} \in V^{(i)} \; \text{and} \; 0 < \left\|x_f - x_f^{(i)}\right\| < \alpha$$

(17)

are checked $\forall\, \boldsymbol{x}_f \in S_f^{(i)}$, the set of simulated fine model points up to the ith iteration. The first condition ensures better coverage by the points in $V^{(i)}$. The second condition rejects points outside an α neighborhood of $\boldsymbol{x}_f^{(i)}$. We denote α as the extraction radius. A point $\boldsymbol{x}_f$ is added to $V^{(i)}$ if (17) is satisfied.

If the $(i-1)$th iteration is unsuccessful, the mapped coarse model should be improved. This is important to guarantee a successful iteration in the ith iteration. However, no improvement is possible if (17) results in $V^{(i)} = V^{(i-1)}$. In this case, an additional perturbation $\Delta\boldsymbol{x}$ is generated by the algorithm. $\Delta\boldsymbol{x}$ is obtained by solving

$$\Delta\boldsymbol{x} = arg\left\{ \min_{\Delta\boldsymbol{x}\in S_v}\ \max_{\boldsymbol{x}_f^{(k)}\in V^{(i)}} \frac{\Delta\boldsymbol{x}^T\left(\boldsymbol{x}_f^{(k)}-\boldsymbol{x}_f^{(i)}\right)}{\left\|\Delta\boldsymbol{x}\right\|\left\|\boldsymbol{x}_f^{(k)}-\boldsymbol{x}_f^{(i)}\right\|} \right\} \tag{18}$$

where

$$S_v = \left\{ \pm\alpha\,\frac{\boldsymbol{v}^{(i)}}{\left\|\boldsymbol{v}^{(i)}\right\|}\,\middle|\, \boldsymbol{J}_f^{(i)T}\boldsymbol{J}_f^{(i)}\boldsymbol{v}^{(i)} = \tau^{(i)}\boldsymbol{v}^{(i)} \text{ and } \tau^{(i)} > 0 \right\} \tag{19}$$

The set S_v contains perturbations of length α in the direction of the eigenvectors of the matrix $\boldsymbol{J}_f^{(i)T}\boldsymbol{J}_f^{(i)}$. A similar approach is utilized by the Aggressive Parameter Extraction (APE) [15] algorithm. These perturbations capture the functional behavior of the fine model within the considered region. $\Delta\boldsymbol{x}$ is a perturbation in S_v that maximizes the coverage of the α-neighbourhood. The point $\boldsymbol{x}_f^{(i)} + \Delta\boldsymbol{x}$ is then simulated and added to $V^{(i)}$. The construction of $V^{(i)}$ is illustrated in Fig. 2.

IV. THE ALGORITHM

The ith iteration of the algorithm proceeds as follows. First, the set $V^{(i)}$ is constructed. The mapping parameters are then estimated using the optimization procedure (15)-(16). The suggested step $\boldsymbol{h}^{(i)}$ is obtained by solving (7), where the surrogate model is given by (8). Notice that (7) utilizes only coarse model simulations and can be solved using traditional optimization methods.

If the response $\boldsymbol{R}_c^*$ is good enough, we may be satisfied with a design for which $\boldsymbol{R}_f(\boldsymbol{x}_f) \approx \boldsymbol{R}_c^*$.

In this case, we select U as $\left\| \boldsymbol{R}_f(\boldsymbol{x}_f) - \boldsymbol{R}_c^* \right\|$. However, if the optimality of the design is the main concern,

U may be selected as the generalized minimax objective function [13].

The optimizer utilized in solving (7) may require first order derivatives in addition to the

surrogate model responses. The surrogate model Jacobian $\boldsymbol{J}_s(\boldsymbol{x}_f^{(i)}) \in \Re^{m \times n}$ is given by

$$\boldsymbol{J}_s(\boldsymbol{x}_f^{(i)}) = \lambda^{(i)} \boldsymbol{J}_m(\boldsymbol{x}_f^{(i)}) + \left(1 - \lambda^{(i)}\right) \boldsymbol{J}_f(\boldsymbol{x}_f^{(i)}) \tag{20}$$

$\boldsymbol{J}_m(\boldsymbol{x}_f^{(i)}) \in \Re^{m \times n}$ is the Jacobian of the mapped coarse model responses at all frequencies. Using (13), it is

given by

$$\boldsymbol{J}_m(\boldsymbol{x}_f^{(i)}) = \left[\boldsymbol{J}_m^T(\boldsymbol{x}_f^{(i)}, \omega_1) \quad \boldsymbol{J}_m^T(\boldsymbol{x}_f^{(i)}, \omega_2) \quad \cdots \quad \boldsymbol{J}_m^T(\boldsymbol{x}_f^{(i)}, \omega_{N_\omega}) \right]^T \tag{21}$$

The step $\boldsymbol{h}^{(i)}$ obtained through (7) is accepted if it improves the fine model objective function.

Otherwise, it is rejected. The parameters $\boldsymbol{J}_f^{(i)}$, $\delta^{(i)}$ and $\lambda^{(i)}$ are updated in every iteration. Broyden's

formula [14] is used to update $\boldsymbol{J}_f^{(i)}$. Initially, we set $\boldsymbol{J}_f^{(1)} = \boldsymbol{J}_c^*$, the Jacobian of the coarse model response

at $\boldsymbol{x}_c^*$. The trust region size $\delta^{(i)}$ is updated based on the ratio between the actual reduction r_a in U and

the predicted reduction r_p. The ratio

$$\rho = \frac{r_a}{r_p} = \frac{U(\boldsymbol{R}_f(\boldsymbol{x}_f^{(i)})) - U(\boldsymbol{R}_f(\boldsymbol{x}_f^{(i)} + \boldsymbol{h}^{(i)}))}{U(\boldsymbol{R}_s^{(i)}(\boldsymbol{x}_f^{(i)})) - U(\boldsymbol{R}_s^{(i)}(\boldsymbol{x}_f^{(i)} + \boldsymbol{h}^{(i)}))} \tag{22}$$

is thus evaluated at the end of each iteration. If $\rho \geq 0.75$, the surrogate model has good accuracy and we

set $\delta^{(i+1)} = \pi_1 \delta^{(i)}$, $\pi_1 > 1.0$. If $\rho \leq 0.10$, we set $\delta^{(i+1)} = \pi_2 \delta^{(i)}$, $0 < \pi_2 < 1.0$. Otherwise, we set $\delta^{(i+1)} = \delta^{(i)}$.

$\lambda^{(i)}$ is updated to favor the more accurate model, either the LFM or the MCM. It is initialized by $\lambda^{(1)} = 1$.

The utilized update is

$$\lambda^{(i+1)} = \frac{\left\| \boldsymbol{E}_l^{(i)} \right\|}{\left\| \boldsymbol{E}_l^{(i)} \right\| + \left\| \boldsymbol{E}_m^{(i)} \right\|} \tag{23}$$

if $E_l^{(i)} \leq \varepsilon_\ell$. Otherwise, we set $\lambda^{(i+1)} = 1$. The vectors $E_m^{(i)} = R_m^{(i)}(x_f^{(i)} + h^{(i)}) - R_f(x_f^{(i)} + h^{(i)})$ and

$E_l^{(i)} = R_f(x_f^{(i)}) + J_f^{(i)} h^{(i)} - R_f(x_f^{(i)} + h^{(i)})$ define the prediction error using the MCM and the LFM,

respectively. The update (23) assigns higher weight to the more accurate model. It should be noted that

the linearized fine model starts with low accuracy. However, Broyden's update iteratively improves the

accuracy of this model. Our algorithm terminates if $n+1$ consecutive unsuccessful iterations are carried

out or if $\left\| h^{(i)} \right\|$ becomes sufficiently small. Fig. 3 illustrates one iteration of the algorithm.

The algorithm can be summarized by the following steps

Step 1. Given $x_f^{(1)} = x_c^*$, $\lambda^{(1)} = 1$, $\delta^{(1)}$, α, $J_f^{(1)} = J_c^*$ and $i=1$.

Step 2. Construct $V^{(i)}$.

Step 3. Apply the optimization procedure (15)-(16) to obtain the mapping parameters.

Step 4. Obtain the suggested step $h^{(i)}$ by solving (7).

Step 5. If $U(R_f(x_f^{(i)} + h^{(i)})) < U(R_f(x_f^{(i)}))$, set $x_f^{(i+1)} = x_f^{(i)} + h^{(i)}$ else $x_f^{(i+1)} = x_f^{(i)}$.

Step 6. Update $J_f^{(i)}$, $\delta^{(i)}$ and $\lambda^{(i)}$.

Step 7. If the stopping criterion is satisfied stop.

Step 8. Set $i=i+1$ and go to Step 2.

A flowchart of the algorithm is shown in Fig. 4.

V. EXAMPLES

A Capacitively-Loaded 10:1 *Impedance Transformer* [10]

We consider the design of a capacitively-loaded 10:1 impedance transformer. The proposed fine and coarse models are shown in Figs. 5 and 6, respectively. The values of the capacitances that we use are given in Table I. Design specifications are

$$|S_{11}| \leq 0.50 \ \text{ for } \ 0.5 \ \text{GHz} \leq \omega \leq 1.5 \ \text{GHz} \tag{24}$$

The electrical lengths of the two transmission lines at 1.0 GHz are selected as designable parameters. The characteristic impedances are kept fixed at the optimal values given in Table II. Both models make use of the ideal transmission line model available in OSA90/hope [16]. Eleven frequency points are simulated per sweep. We utilized the real and imaginary parts of S_{11} in the optimization procedure (15)-(16). The initial trust region size and extraction radius are $\delta^{(1)} = 0.09 \|x_c^*\|_\infty$ and $\alpha = 0.09 \|x_c^*\|_\infty$, respectively. The algorithm executed five iterations. Only the first two are successful. The total number of fine model simulations is seven. The initial and final designs are given in Table III. The corresponding responses are shown in Figs. 7 and 8, respectively. The final mapping is given by

$$\boldsymbol{B}^{(6)} = \begin{bmatrix} 1.12886 & 0.19245 \\ -0.17669 & 1.19167 \end{bmatrix}, \ \boldsymbol{c}^{(6)} = \begin{bmatrix} 84.52643 \\ 87.95123 \end{bmatrix}, \ \boldsymbol{s}^{(6)} = \begin{bmatrix} -0.06863 \\ 0.06035 \end{bmatrix},$$

$$\boldsymbol{t}^{(6)} = \begin{bmatrix} -0.00026 \\ -0.00212 \end{bmatrix}, \ \sigma^{(6)} = 1.03243 \text{ and } \gamma^{(6)} = 0.00983 \tag{25}$$

The value of *U* in every iteration is shown in Fig. 9.

A Double-Folded Stub (*DFS*) *Filter* [11]

The DFS fine model utilizes Sonnet's *em* [17] through Empipe [16] (See Fig. 10). The coarse model, shown in Fig. 11, exploits the microstrip line and microstrip T-junction models available in OSA90/hope. The coupling between the folded stubs and the microstrip line is simulated using equivalent capacitors. The values of these capacitors are determined using Walker's formulas [18]. Jansen's microstrip bend model [19] is used to model the folding effect of the stub.

The design specifications are

$$|S_{21}| \geq -3 \text{ dB} \text{ for } \omega \leq 9.5 \text{ GHz} \text{ and } 16.5 \text{ GHz} \leq \omega$$

$$|S_{21}| \leq -30 \text{ dB} \text{ for } 12 \text{ GHz} \leq \omega \leq 14 \text{ GHz}$$

(26)

L_1, L_2 and S are selected as designable parameters. W_1 and W_2 are fixed at 4.8 mil. Only eleven frequency points are utilized per sweep. The mapping parameters are obtained using the real and imaginary parts of S_{21}. The initial trust region size and extraction radius are $\delta^{(1)} = 0.09 \|x_c^*\|_\infty$ and $\alpha = 0.09 \|x_c^*\|_\infty$. The width S is scaled by a factor of 6.0 to make the problem better conditioned.

The design procedure is carried out with the interpolation option of Empipe disabled. Here, every iterate is snapped to the nearest on-grid point. Our algorithm carried out only 16 iterations. A total of 18 calls to Empipe (18 *em* simulations) were needed. The initial and final designs are given in Table IV. The corresponding responses are shown in Figs. 12 and 13. The value of U in each iteration is shown in Fig. 14. The final mapping parameters are

$$\boldsymbol{B}^{(17)} = \begin{bmatrix} 1.03074 & 0.11174 & 0.00031 \\ -0.20595 & 0.96384 & 0.00365 \\ -0.35144 & 0.34204 & 0.78257 \end{bmatrix}, \boldsymbol{c}^{(17)} = \begin{bmatrix} 236.1134 \\ 21.5218 \\ 74.8218 \end{bmatrix}, \boldsymbol{s}^{(17)} = \begin{bmatrix} 0.44639 \\ 0.70939 \\ 0.50045 \end{bmatrix},$$

(27)

$$\boldsymbol{t}^{(17)} = \begin{bmatrix} 0.03854 \\ -0.01167 \\ 0.00439 \end{bmatrix}, \sigma^{(17)} = 1.13771 \text{ and } \gamma^{(17)} = -0.55168$$

The HTS Filter

We also consider the design of an HTS filter [12]. This filter is shown in Fig. 15. The design specifications are

$$|S_{21}| \leq 0.05 \text{ for } \omega \leq 3.967 \text{ GHz} \text{ and } 4.099 \text{ GHz} \leq \omega$$

$$|S_{21}| \geq 0.95 \text{ for } 4.008 \text{ GHz} \leq \omega \leq 4.058 \text{ GHz}$$

(28)

The designable parameters are L_1, L_2, L_3, S_1, S_2 and S_3. We take $L_0 = 50$ mil and $W = 7$ mil. The coarse model exploits the empirical models of microstrip lines, coupled lines and open stubs available in OSA90/hope (see Fig. 16). The fine model employs Sonnet's *em* through Empipe. We utilized the real

and imaginary parts of both S_{11} and S_{21} in the optimization procedure (15)-(16). The initial trust region size is $\delta^{(1)} = 0.20 \left\| x_c^* \right\|_\infty$. The α-neighborhood is selected as an n-dimensional box. This takes into account that the response is more sensitive to the lengths than the widths. The interpolation option of Empipe is disabled to make the optimization time reasonable.

Here, we fix $s^{(i)} = t^{(i)} = 0$. The rest of the mapping parameters are obtained using (15)-(16). This implies that the frequency and space mappings are decoupled. This approach reduces the number of optimizable parameters in (15)-(16). Consequently, it makes the extraction of the mapping parameters better conditioned. This approach is motivated by the fact that previous examples have effectively decoupled mappings ($s^{(i)} \approx 0$ and $t^{(i)} \approx 0$).

The HTS design is carried out assuming lossless substrate dielectric. A relatively coarse grid size is used. The material and physical parameters values used in both OSA90/hope and in *em* are shown in Table V. The fine model is simulated at 16 frequency points per sweep. Starting from the snapped optimal coarse design, the final design is reached in 7 iterations only. A total of 7 fine model simulations are used. The initial and final designs are given in Table VI. The corresponding responses are shown in Figs 17 and 18, respectively. The value of U in each iteration is shown in Fig. 19.

Fig. 20 illustrates the fine model response at the end of the first iteration. It is seen that the fine model response is well aligned in the proper band using only one fine model simulation. This illustrates the power of the algorithm in handling significant frequency shifts. The final mapping is given by

$$
B^{(8)} = \begin{bmatrix}
1.08894 & 0.00855 & -0.01082 & 0.01422 & -0.07505 & -0.00979 \\
-0.00481 & 0.96627 & -0.00695 & 0.00912 & -0.03234 & -0.00592 \\
0.00828 & -0.00831 & 0.97551 & -0.01433 & 0.02963 & 0.00955 \\
-0.01513 & 0.01509 & -0.02016 & 1.04437 & 0.01671 & -0.01747 \\
-0.01324 & 0.01320 & -0.01766 & 0.02317 & 1.03175 & -0.01541 \\
-0.01401 & 0.01400 & -0.01869 & 0.02453 & 0.00672 & 0.95969
\end{bmatrix},
$$

(29)

$$\boldsymbol{c}^{(8)} = \begin{bmatrix} 180.61046 \\ 190.38887 \\ 180.53859 \\ 23.96889 \\ 98.89007 \\ 113.32096 \end{bmatrix}, \quad \boldsymbol{t}^{(8)} = \boldsymbol{s}^{(8)} = \boldsymbol{0}, \quad \sigma^{(8)} = 1.07264, \quad \gamma^{(8)} = -0.12873$$

VI. CONCLUSIONS

We present a breakthrough algorithm for efficient optimization of microwave circuits. The algorithm integrates, for the first time, SM optimization with surrogate model optimization. It exploits a surrogate model in the form of a convex combination of a mapped coarse model and a linearized fine model. The MCM utilizes a novel frequency-space mapping. During optimization, the coarse and fine models are simulated over different frequency ranges. This approach is shown to be powerful, especially if significant response shift exists. It also enables indirect estimation of the derivatives of fine model responses. The algorithm is successfully illustrated through the design of microwave filters and transformers.

REFERENCES

[1] M.H. Bakr, J.W. Bandler, K. Madsen, J.E. Rayas-Sánchez and J. Søndergaard, "Space mapping optimization of microwave circuits exploiting surrogate models," *IEEE MTT-S Int. Microwave Symp. Dig*. (Boston, MA), 2000, pp. 1785-1788.

[2] J.W. Bandler, R.M. Biernacki, S.H. Chen, R.H. Hemmers and K. Madsen, "Electromagnetic optimization exploiting aggressive space mapping," *IEEE Trans. Microwave Theory Tech.*, vol. 43, 1995, pp. 2874-2882.

[3] M.H. Bakr, J.W. Bandler, R.M. Biernacki, S.H. Chen and K. Madsen, "A trust region aggressive space mapping algorithm for EM optimization," *IEEE Trans. Microwave Theory Tech.*, vol. 46, 1998, pp. 2412-2425.

[4] M.H. Bakr, J.W. Bandler, N. Georgieva and K. Madsen, "A hybrid aggressive space mapping algorithm for EM optimization," *IEEE Trans. Microwave Theory Tech.*, vol. 47, 1999, pp. 2440-2449.

[5] A.J. Booker, J.E. Dennis, Jr., P.D. Frank, D. B. Serafini, V. Torczon and M.W. Trosset, "A rigorous framework for optimization of expensive functions by surrogates," *Structural Optimization*, vol. 17, 1999, pp. 1-13.

[6] V. Torczon and M.W. Trosset, "Using approximations to accelerate engineering design optimization," *Technical Report* 98-33, *ICASE*, Langley Research Center, Hampton, Virginia 23681-2199, 1998.

[7] N. Alexandrov, J.E. Dennis, Jr., R.M. Lewis and V. Torczon, "A trust region framework for managing the use of approximation models in optimization," *Structural Optimization*, vol. 15, 1998, pp. 16-23.

[8] J.W. Bandler, M.A. Ismail, J.E. Rayas-Sánchez and Q.J. Zhang, "Neuromodeling of microwave circuits exploiting space mapping technology," *IEEE Trans. Microwave Theory Tech.*, vol. 47, 1999, pp. 2417-2427.

[9] J.W. Bandler, N. Georgieva, M.A. Ismail, J.E. Rayas-Sánchez and Q. J. Zhang, "A generalized space mapping tableau approach to device modeling," 29th *European Microwave Conf.* (Munich, Germany), 1999, vol. 3, pp. 231-234.

[10] J.W. Bandler, "Optimization methods for computer-aided design," *IEEE Trans. Microwave Theory Tech.*, vol. MTT-17, 1969, pp. 533-552.

[11] J.C. Rautio, Sonnet Software, Inc., 1020 Seventh North Street, Suite 210, Liverpool, NY 13088, Private Communication, 1992.

[12] J.W. Bandler, R.M. Biernacki, S.H. Chen, W.J. Gestinger, P.A. Grobelny, C. Moskowitz and S.H. Talisa, "Electromagnetic design of high-temperature superconducting filters," *Int. J. Microwave and Millimeter-Wave Computer-Aided Engineering*, vol. 5, 1995, pp. 331-343.

[13] J.W. Bandler, W. Kellermann and K. Madsen, "A superlinearly convergent minimax algorithm for microwave circuit design," *IEEE Trans. Microwave Theory Tech*., vol. MTT-33, 1985, pp. 1519-1530.

[14] C.G. Broyden, "A class of methods for solving nonlinear simultaneous equations," *Math. Comp.*, vol. 19, 1965, pp. 577-593.

[15] M.H. Bakr, J.W. Bandler and N. Georgieva, "An aggressive approach to parameter extraction," *IEEE Trans. Microwave Theory Tech.*, vol. 47, 1999, pp. 2428-2439.

[16] OSA90/hope™ and Empipe™, Version 4.0, formerly Optimization Systems Associates Inc., P.O. Box 8083, Dundas, ON, Canada, L9H 5E7, 1997, now Agilent Technologies, 1400 Fountaingrove Parkway, Santa Rosa, CA 95403-1799.

[17] *em*™ , Sonnet Software, Inc., 1020 Seventh North Street, Suite 210, Liverpool, NY 13088, 1997.

[18] C.S. Walker, *Capacitance, Inductance and Crosstalk Analysis*. Norwood, MA: Artech House, 1990.

[19] M. Kirschning, R. Jansen and N. Koster, "Measurement and computer-aided modeling of microstrip discontinuities by an improved resonator method," *IEEE MTT-S Int. Microwave Symp. Dig*. (Boston, MA), 1983, pp. 495-497.

TABLE I
THE FINE MODEL CAPACITANCES FOR THE
CAPACITIVELY-LOADED IMPEDANCE
TRANSFORMER

Capacitance	Value
C_1	10
C_2	10
C_3	10
all values are in pF	

TABLE II
THE CHARACTERISTIC IMPEDANCES FOR
THE CAPACITIVELY-LOADED IMPEDANCE
TRANSFORMER

Impedance	Value
Z_1	2.23615
Z_2	4.47230
all values are in ohm	

TABLE III
THE INITIAL AND FINAL DESIGNS FOR THE
CAPACITIVELY-LOADED IMPEDANCE
TRANSFORMER

Parameter	$x_f^{(1)}$	$x_f^{(6)}$
L_1	90.0000	81.59880
L_2	90.0000	74.38324
all values are in degrees		

TABLE IV

THE INITIAL AND FINAL DESIGNS FOR THE
DFS FILTER

Parameter	$x_f^{(1)}$	$x_f^{(17)}$
S	9.60	6.4
L_2	60.80	84.8
L_1	67.2	86.4

all values are in mil

TABLE V
MATERIAL AND PHYSICAL PARAMETERS
FOR THE HTS FILTER

Model Parameter	OSA90/hope	*em*
substrate dielectric constant	23.425	23.425
substrate thickness (mil)	19.9516	19.9516
shielding cover height (mil)	∞	250
Conducting material thickness	0	0
Substrate dielectric loss tangent	0	0
Resistivity of metal (Ωm)	0	0
Surface roughness of metal	0	—
Magnetic loss tangent	—	0
Surface reactance (Ω/sq)	—	0
x-grid cell size (mil)	—	1.00
y-grid cell size (mil)	—	1.75

TABLE VI
THE INITIAL AND FINAL DESIGNS FOR
THE HTS FILTER

Parameter	$x_f^{(1)}$	$\mathbf{x}_f^{(8)}$
L_1	188.00	188.00
L_2	198.00	192.00
L_3	189.00	187.00
S_1	22.75	22.75
S_2	99.75	78.75
S_3	112.00	91.00

all values are in mils
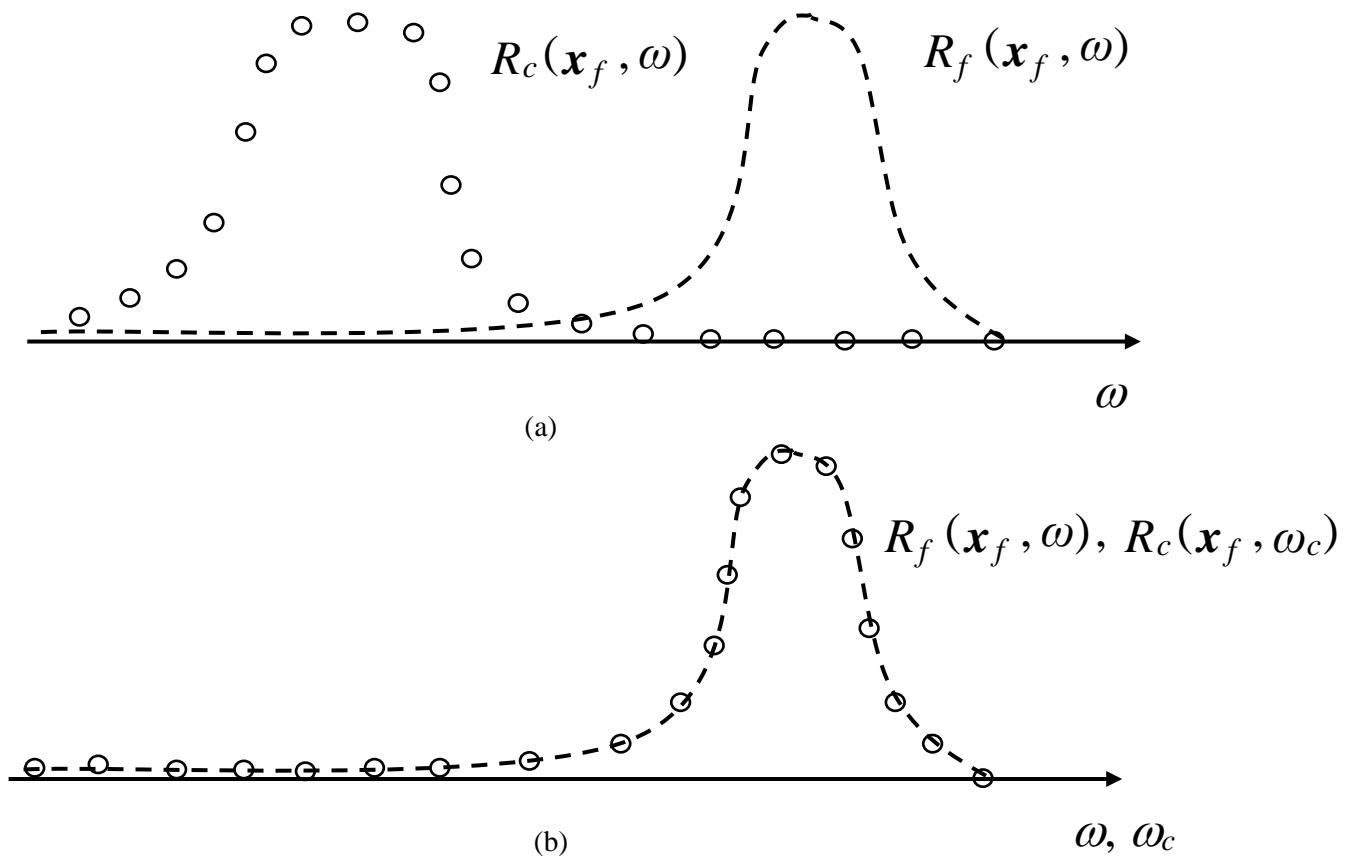
Fig. 1. Illustration of the frequency-sensitive mapping concept, (a) a significant frequency band shift exists between fine and coarse model responses at the initial iteration and (b) the coarse model frequency is transformed such that both responses match.
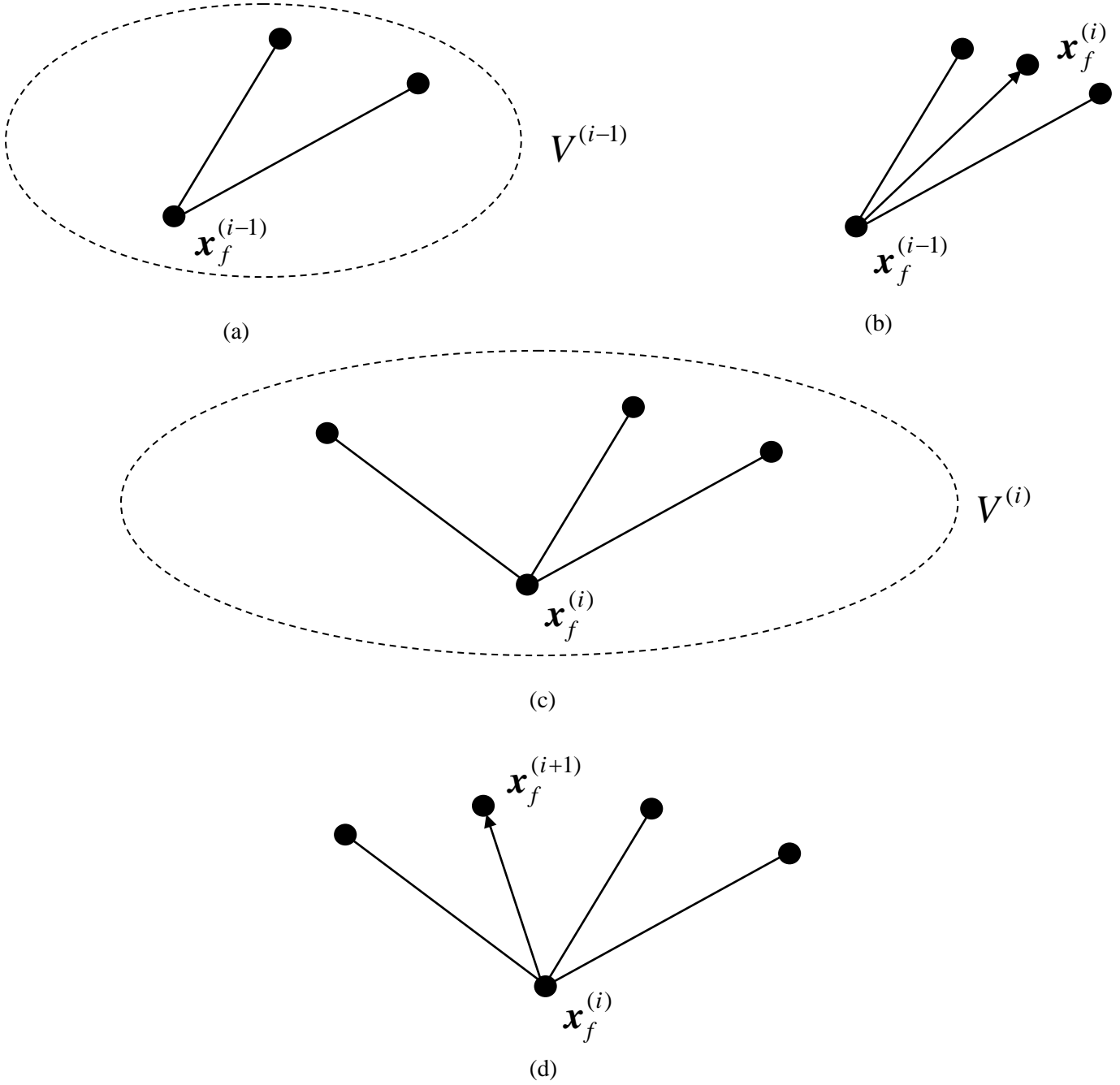
Fig. 2. Illustration of the selection of the parameter extraction points, (a) at the $(i-1)$th iteration, we have the point $\boldsymbol{x}_f^{(i-1)}$ and the set $V^{(i-1)}$, (b) a new point is generated by the algorithm that does not satisfy the success criterion, (c) $\boldsymbol{x}_f^{(i-1)}$ becomes $\boldsymbol{x}_f^{(i)}$, the previous perturbation $\boldsymbol{h}^{(i)}$ is excluded from $V^{(i)}$ and the algorithm generates an alternative perturbation and (d) the set $V^{(i)}$ is used to extract new mapping parameters and predict a successful iterate.
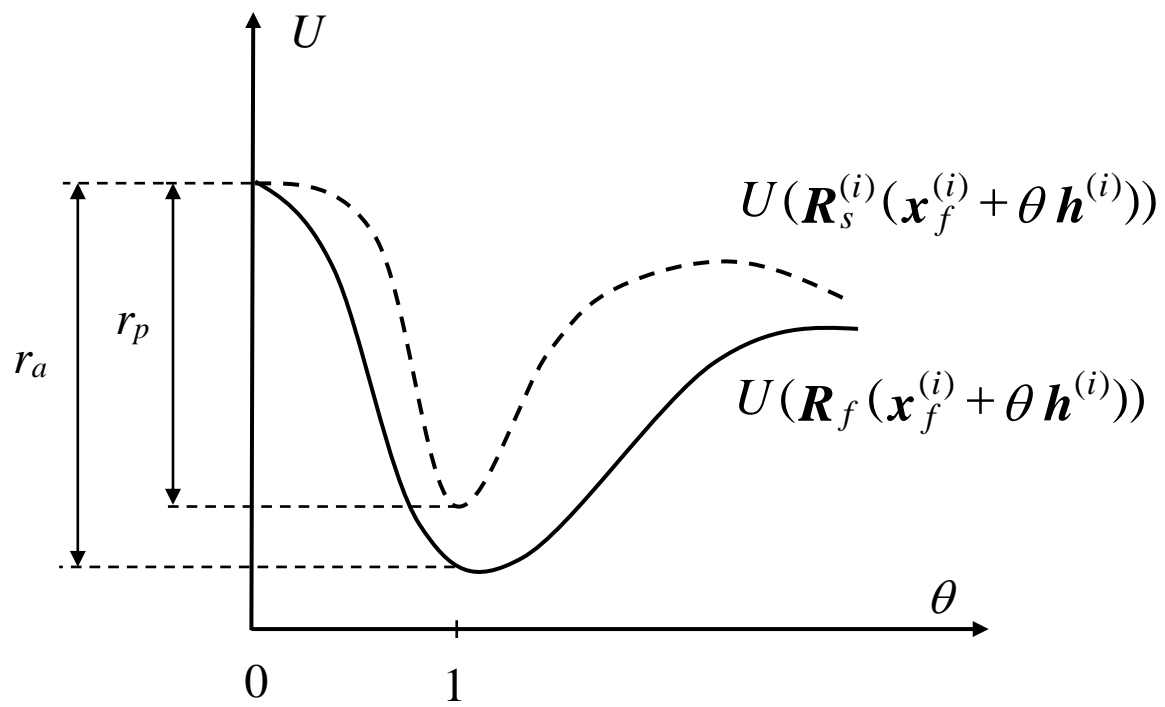
Fig. 3. Illustration of the *i*th iteration of the algorithm.
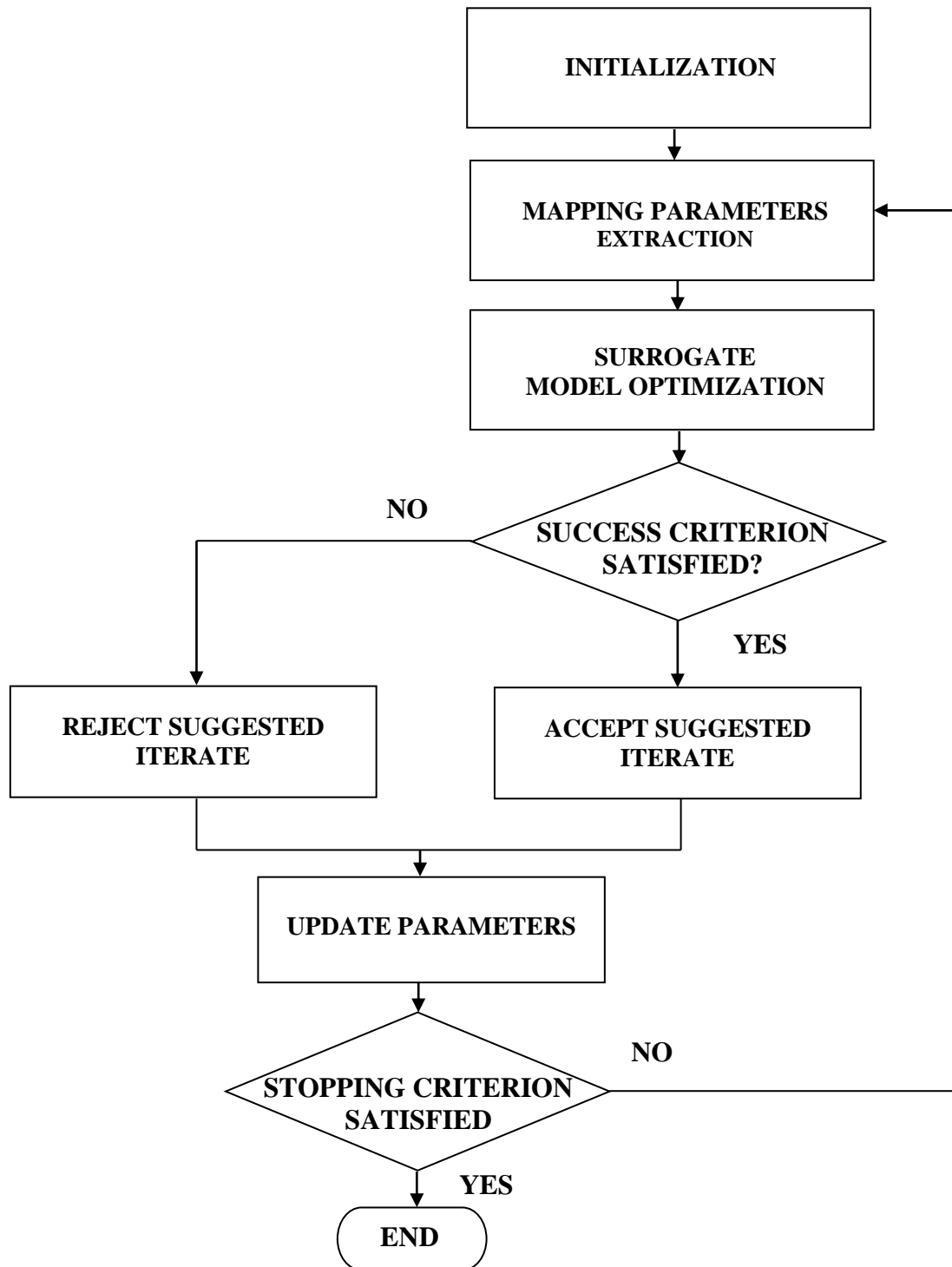
Fig. 4. A flowchart of the algorithm.
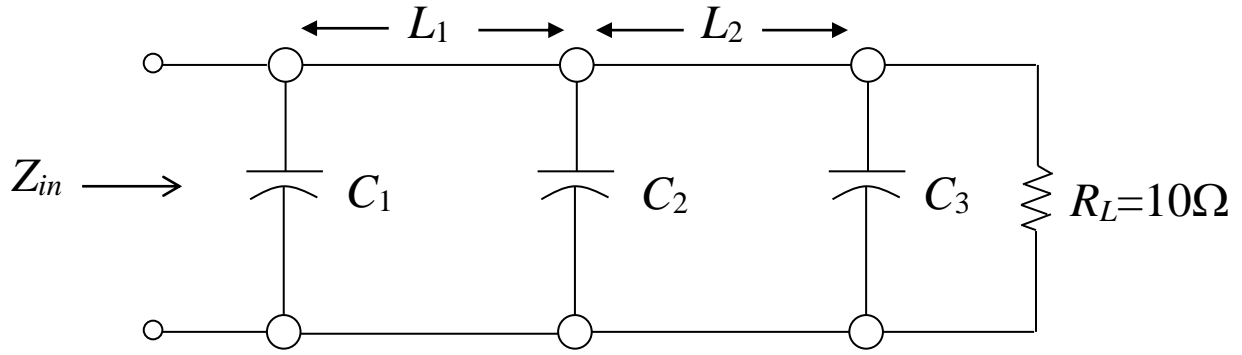
Fig. 5. The fine model of the capacitively-loaded 10:1 impedance transformer.
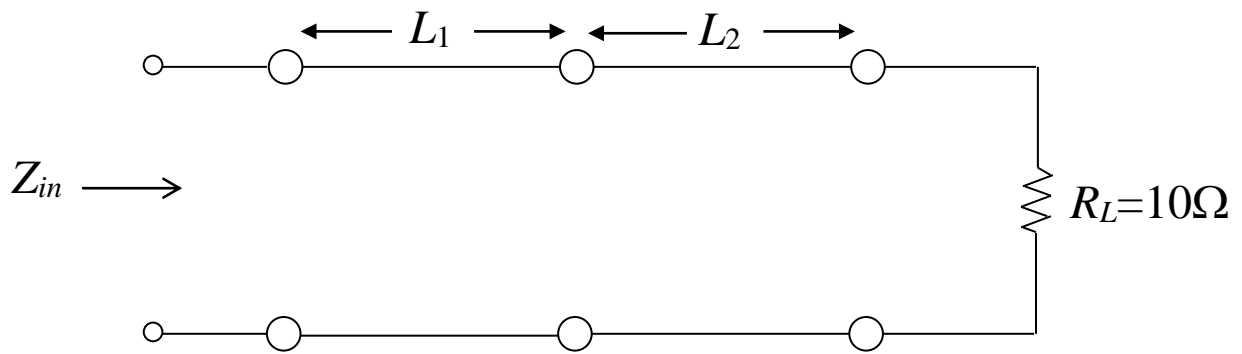
Fig. 6. The coarse model of the capacitively-loaded 10:1 impedance transformer.
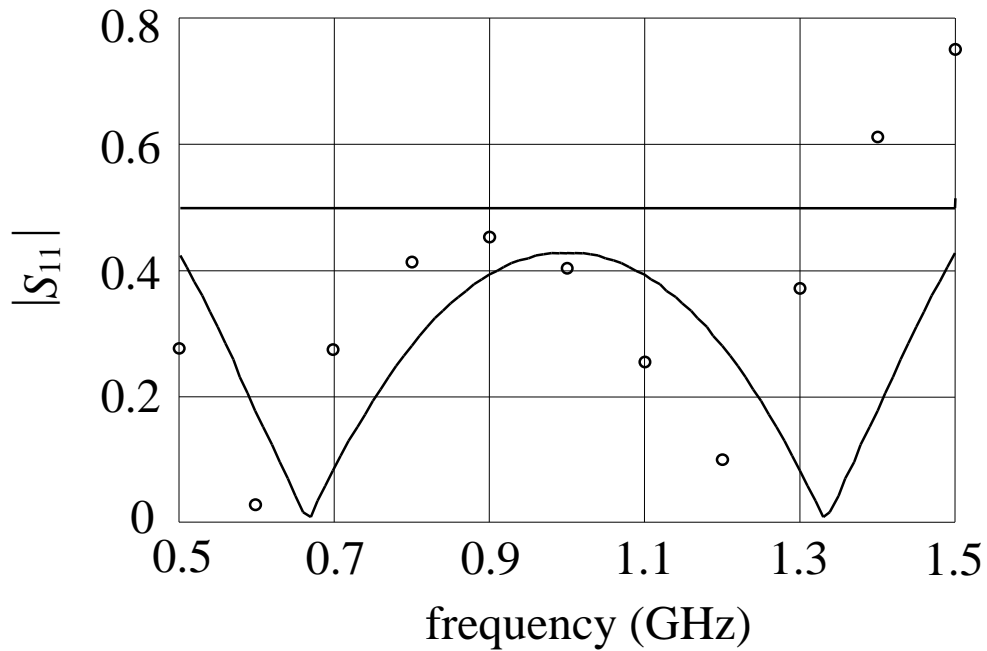
Fig. 7. The optimal coarse model response (——) and the fine model response (o) at the starting point for the capacitively-loaded 10:1 impedance transformer.
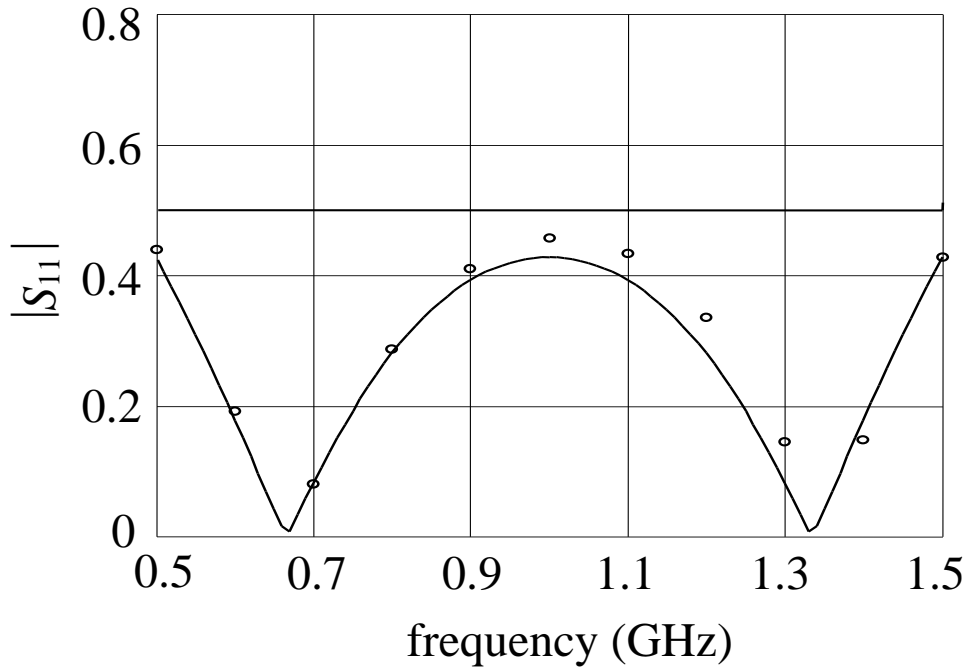
Fig. 8. The optimal coarse model response (—) and the fine model response (o) at the final design for the capacitively-loaded 10:1 impedance transformer.
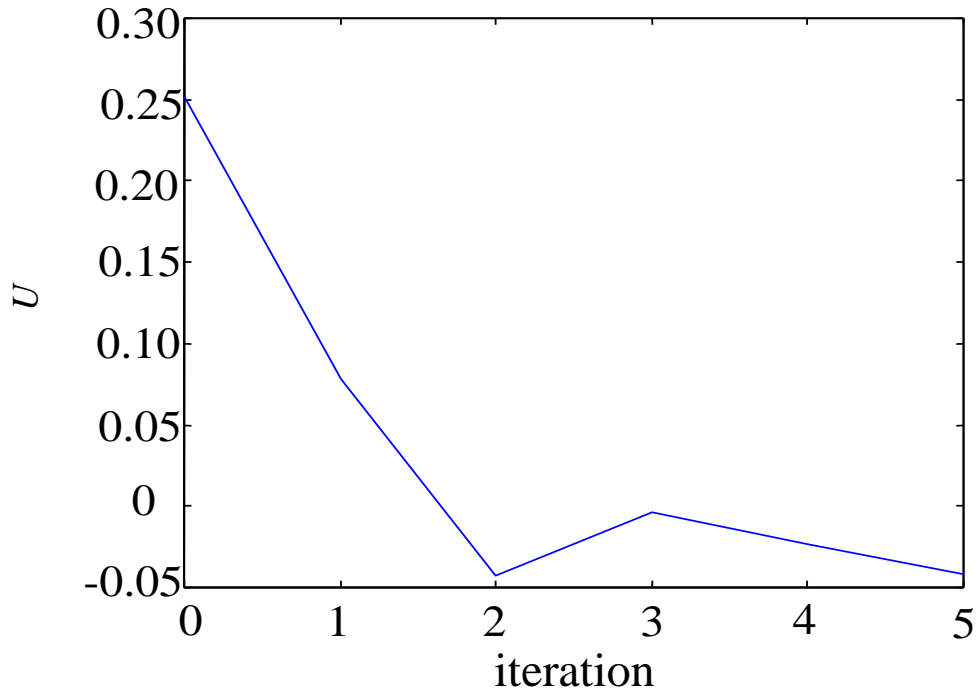
Fig. 9. The value of *U* in each iteration for the 10:1 impedance transformer.
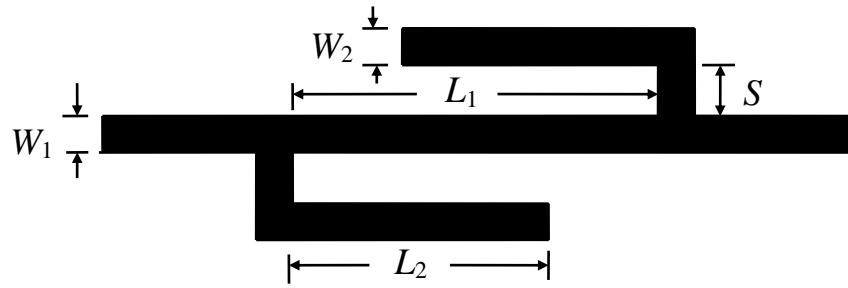
Fig. 10. The DFS filter.
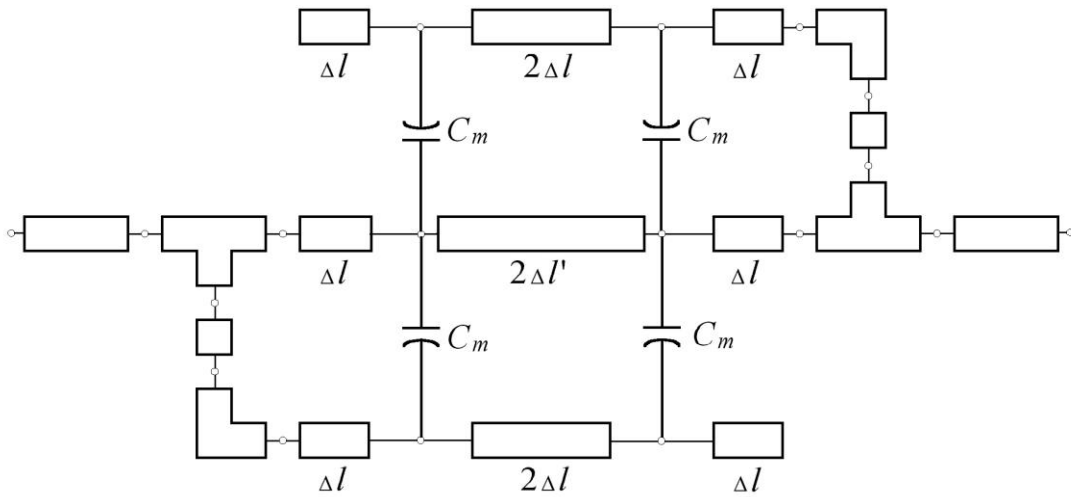
Fig. 11. The coarse model of the DFS filter.
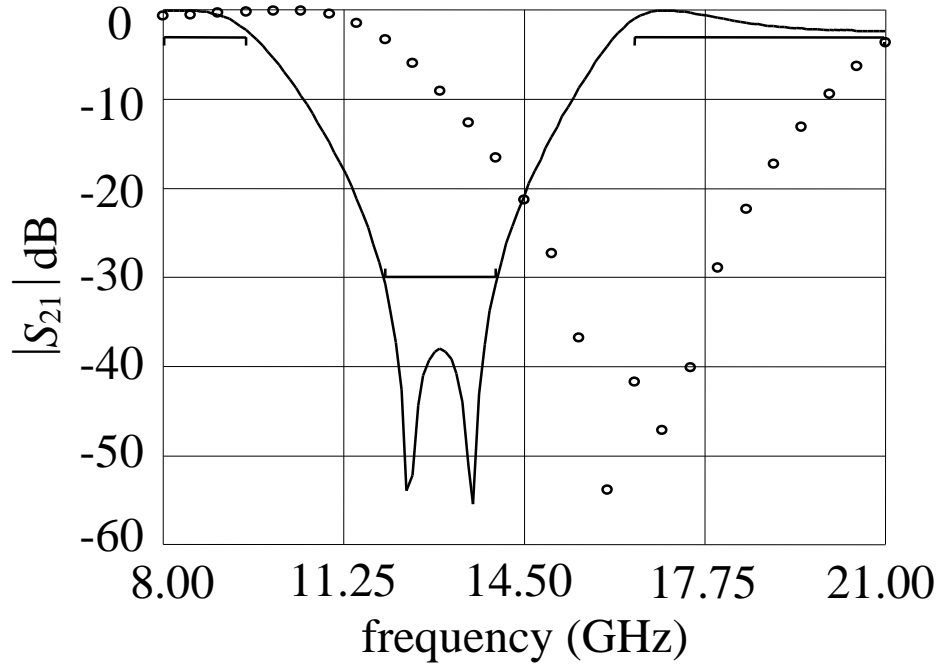
Fig. 12. The optimal coarse model response (—) and the fine model response (o) at the starting design for the DFS filter.
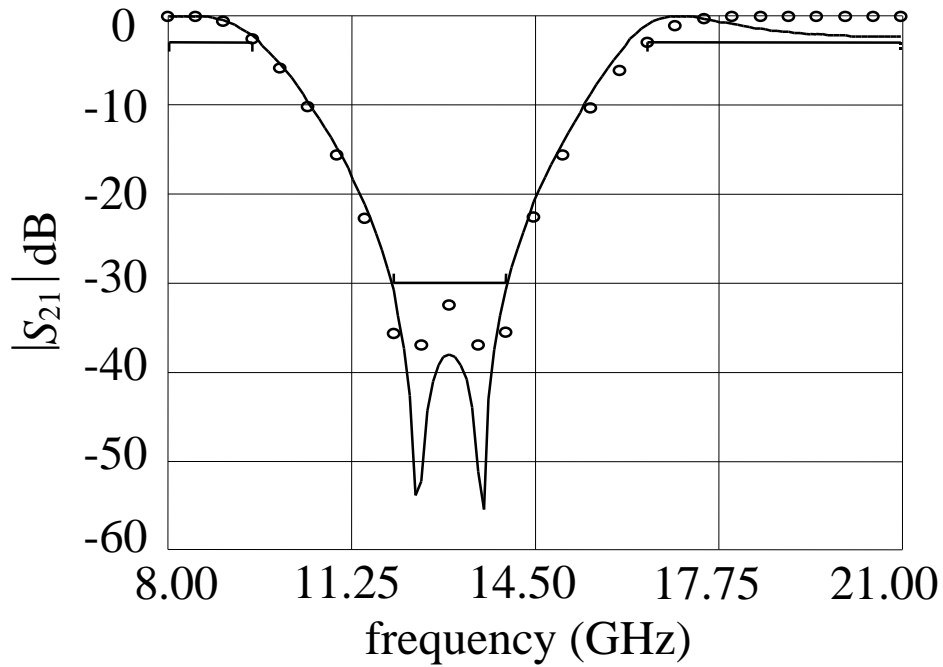
Fig. 13. The optimal coarse model response (—) and the fine model response (o) at the final design for the DFS filter.

26
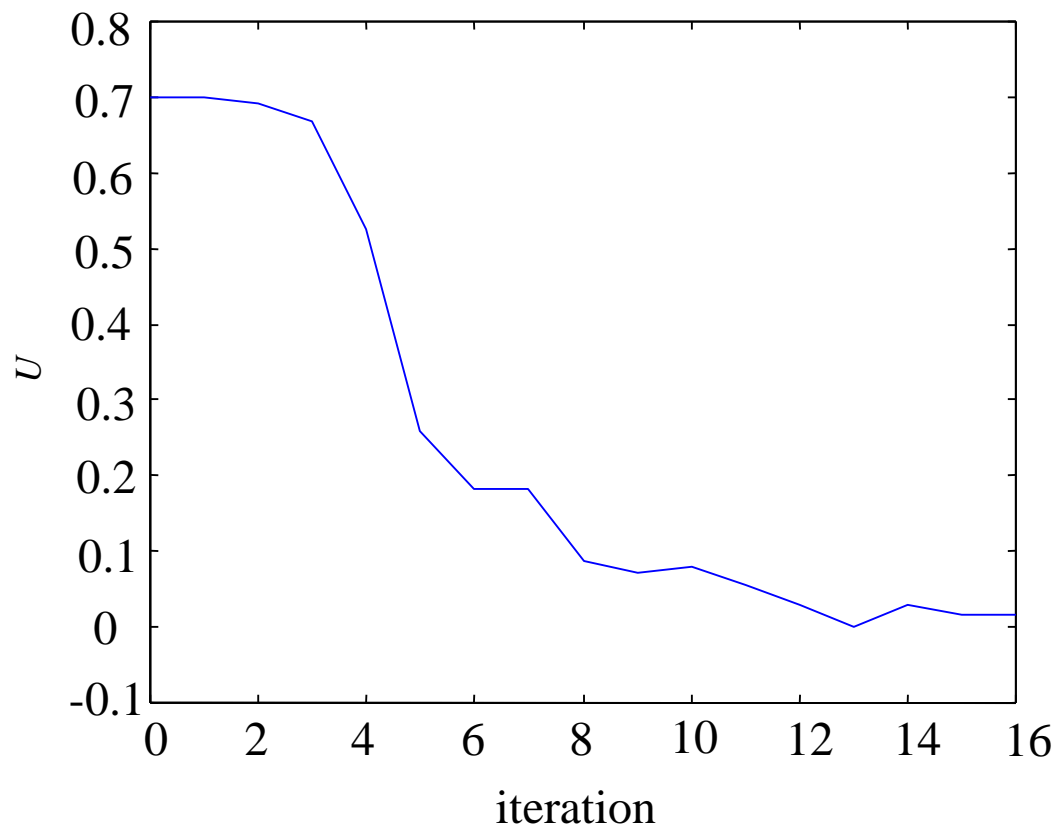
Fig. 14. The value of U at every iteration for the DFS filter.
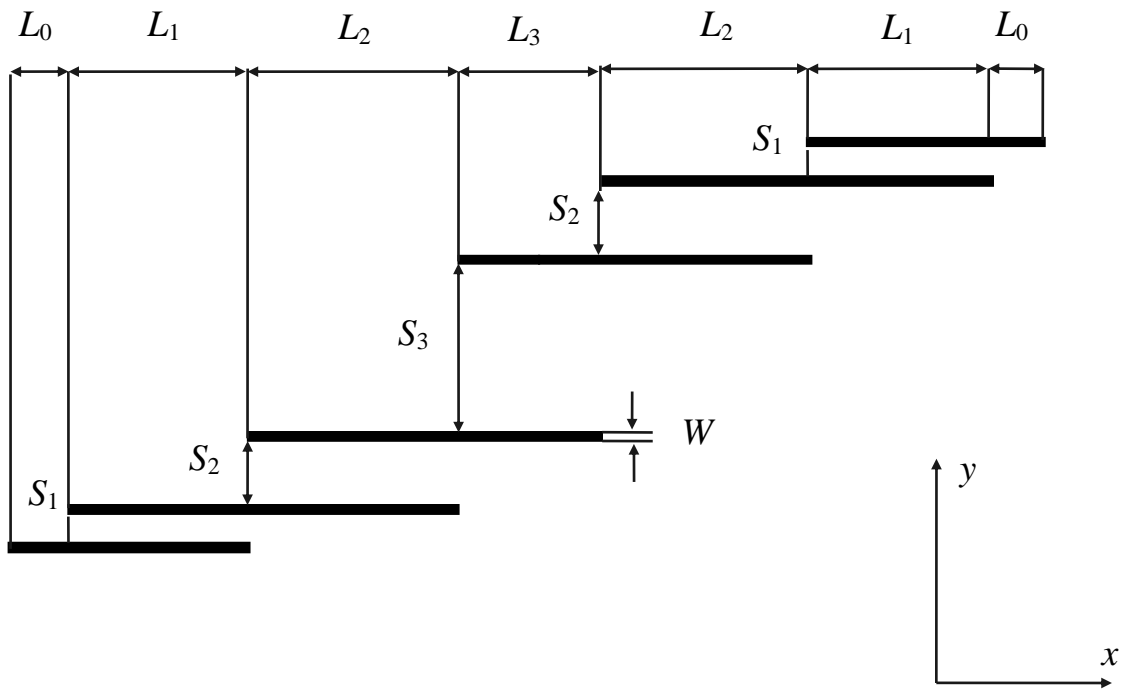
Fig. 15. The HTS filter.
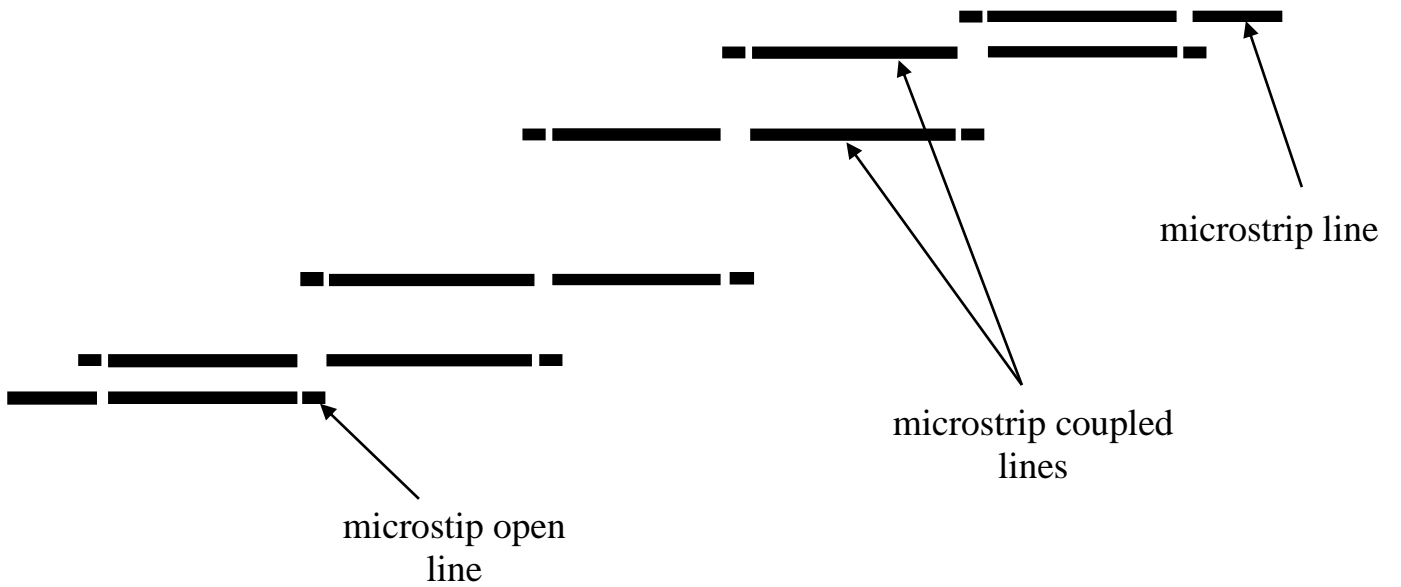
Fig. 16. The coarse model of the HTS filter.
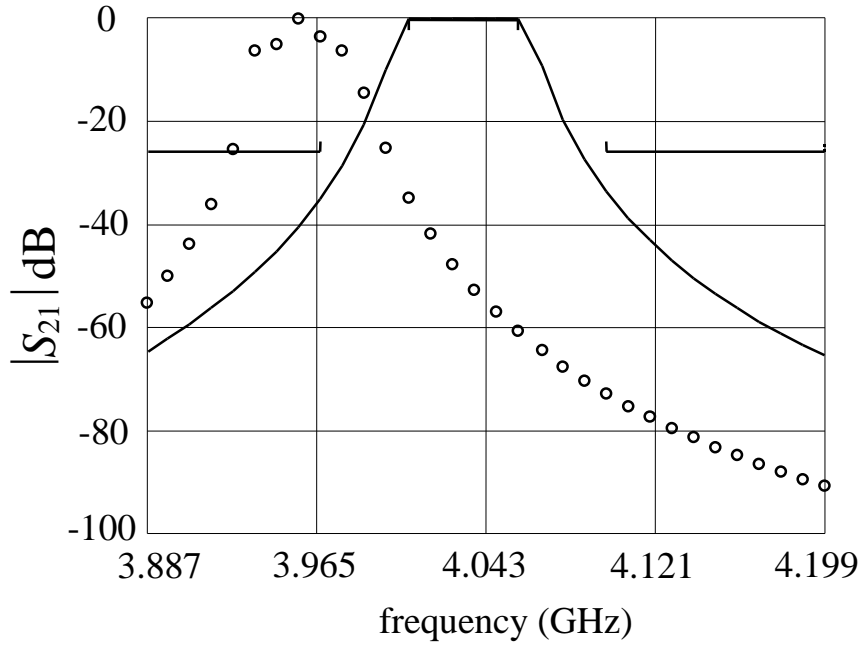
Fig. 17. The optimal coarse model response (—) and the fine model response (o) at the initial design for the HTS filter.
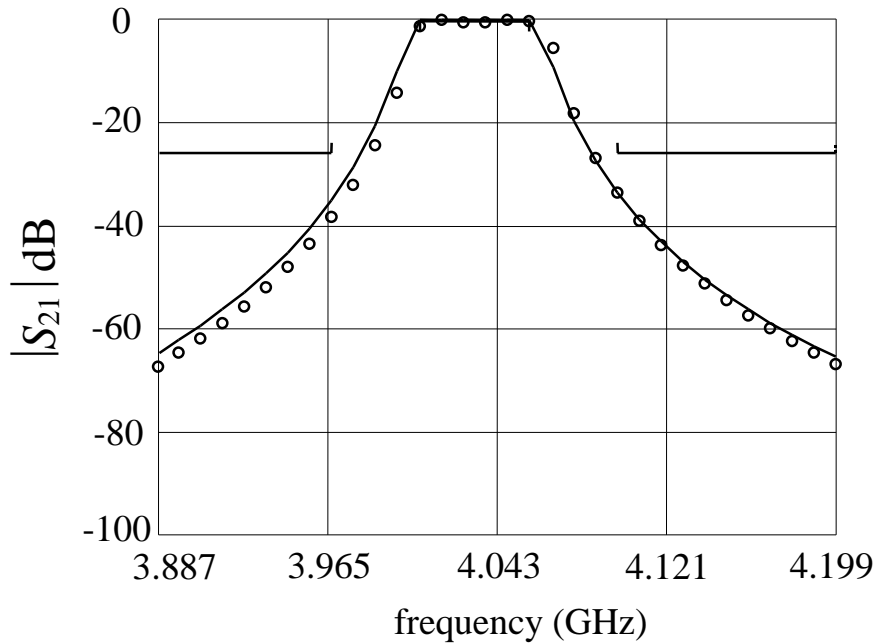
Fig. 18. The optimal coarse model response (—) and the fine model response (o) at the final design for the HTS filter.
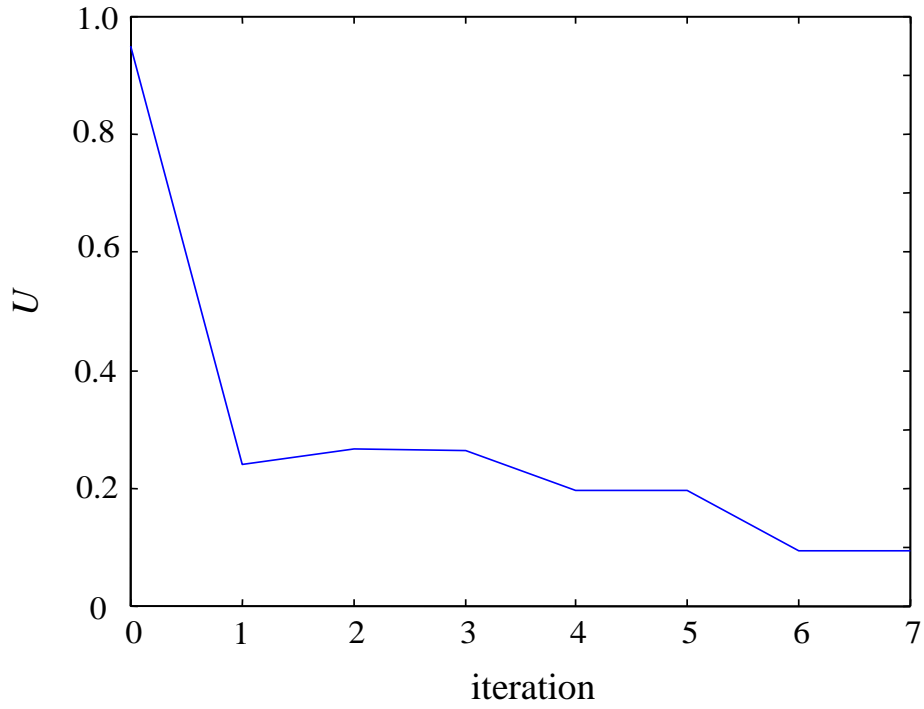
Fig. 19. The value of U at every iteration for the HTS filter.
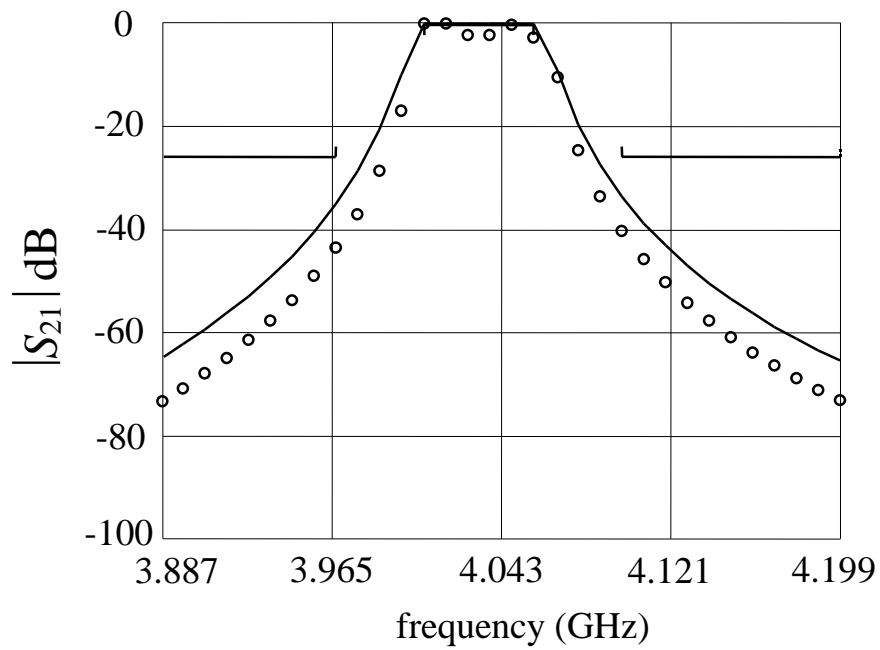
Fig. 20. The optimal coarse model response (——) and the fine model response (o) at the end of the first iteration for the HTS filter.